Room-Temperature Reversible Chemisorption of Carbon Monoxide on Nickel(0) Complexes

Yasuhiro Yamauchi[1], Yoichi Hoshimoto[1]*, Takahiro Kawakita[1], Takuya Kinoshita[1], Yuta Uetake[1,2], Hidehiro Sakurai[1,2], Sensuke Ogoshi[1]*

Affiliations

[1]Department of Applied Chemistry, Faculty of Engineering, Osaka University, Suita, Osaka 565-0871, Japan.

[2]Innovative Catalysis Science Division, Institute for Open and Transdisciplinary Research Initiatives (ICS-OTRI), Osaka University, Suita, Osaka 565-0871, Japan.

*Correspondence to: hoshimoto@chem.eng.osaka-u.ac.jp; ogoshi@chem.eng.osaka-u.ac.jp

Abstract

Chemisorption on organometallic-based adsorbents is crucial for the controlled separation and long-term storage of gaseous molecules. The formation of covalent bonds between the metal centers in the adsorbents and the targeted gases affects the desorption efficiency, especially when the oxidation state of the metal is low. Herein, we report a pressure-responsive nickel(0)-based system that is able to reversibly chemisorb carbon monoxide (CO) at room temperature. The use of *N*-heterocyclic carbene ligands with hemi-labile *N*-phosphine oxide substituents facilitates both the adsorption and desorption of CO on nickel(0) via ligand substitution. Ionic liquids were used as the reaction medium to enhance the desorption rate and establish a reusable system. These results showcase a way for the sustainable chemisorption of CO using a zero-valent transition-metal complex.

One-Sentence Summary

A reusable, reversible pressure-responsive CO chemisorption system based on a Ni(0) complex in ionic liquids is reported.

Main Text

Carbon monoxide (CO) is an essential feedstock that is widely used in the synthesis of commodity chemicals such as alcohols, carboxylic acids, and polycarbonates (*1*). CO has also been used for metal-refining processes, e.g., the Mond process, which consists of the carbonylation of crude Ni(0) at around 50 °C and thermolysis of gaseous $Ni(CO)_4$ at 180–280 °C (*2*,*3*). Huge amounts of high-purity CO are thus produced during the removal of contaminants such as H_2, N_2, CO_2, and CH_4 from crude materials obtained from the gasification processes of hydrocarbon resources (*1*) and the steel production industry (*4*). In these cases, cryogenic distillation technology is typically applied for CO purification, although technologies based on adsorption, absorption, and membranes have also been explored intensively (*4*,*5*). In terms of the purity of the produced CO, repeatable adsorption/desorption sequences based on the coordination/dissociation of CO on metal ions such as Fe(II) (*6*-*8*), Co(II) (*8*,*9*), Ni(II) (*10*), Cu(I) (*11*), Cu(II) (*12*), and Ir(III) (*13*) incorporated in solid-state adsorbents have shown exceptional results (Fig. 1A). For example, Kirschner et al. reported the use of the crystalline solid of a Fe(II)-carbonyl complex that bears a PNP pincer-type ligand for the reversible chemisorption of CO (*6*). In this reaction, the adsorption proceeded smoothly under ambient conditions, while the efficient desorption required heating (100 °C) under reduced pressure. The crystalline coordination polymers known as metal–organic frameworks (MOFs) have also been used for the purification of CO (*5*,*14*). Matsuda and Kitagawa et al. demonstrated the separation of CO from a gaseous mixture including nitrogen (N_2), which is the most competitive gas for CO in physisorption-based separation processes due to its similar molecular size, using a Cu(II)-based nanoporous crystalline material; this separation was enabled by the coordination of CO to Cu(II) ions under cryogenic conditions (*12*). In this report, desorption was carried out by raising the temperature to 27 °C in a closed system that had undergone a single degassing cycle. Similarly, Long et al. proposed the application of Fe(II)-, Co(II)-, and Ni(II)-based MOFs for the purification of CO based on their high susceptibility to adsorb CO (*10*,*15*). Various metal-containing sorbents dispersed in activated carbons, zeolite, and silica have also been proven to be potential materials for CO purification (*5*,*16*-*19*); however, these are usually associated with higher costs and lower metal density compared to molecular-based systems and MOFs. Given the significant impact of purification processes on capital and operating costs in industry (accounting for 40–70%) and on global energy consumption (accounting for 10–15%) (*20*), the establishment of a novel strategy for less-energy-consuming and sustainable chemisorption systems is desirable.

To design such systems for CO purification, the affinity between the metal and CO is a central point of consideration (Fig. 1B). In principle, more rapid and selective adsorption of CO can be achieved by the introduction of low- (or zero-) valent, *d*-electron-rich metals, as such metals can form thermodynamically favorable metal–CO interactions through their stronger metal-to-CO π-backdonation compared to higher-valent metals (*21*,*22*). However, the strong interaction between low-valent metals and CO greatly affects the desorption efficiency. In fact, the reversible chemisorption of CO with zero-valent transition metals has been achieved under the extreme conditions used in the Mond process (*vide supra*). Thus, hitherto reported adsorption technologies have predominantly relied on the chemisorption of CO by higher-valent metals to minimize the influence of metal-to-CO π-backdonation. Temperature-swing operations, i.e., the use of a higher operation temperature during CO desorption than during CO adsorption, are frequently applied, and desorption is often carried out under reduced pressure (pressure-swing operation) (*6*,*8*,*9*,*12*,*13*,*15*). Against this background, we envisioned the development of a process for the reversible chemisorption of CO using a zero-valent transition metal that could potentially exhibit

strong metal-to-CO π-backdonation to showcase a novel strategy for the controlled purification and long-term storage of CO.

Herein, we present a method for the reversible pressure-swing chemisorption of CO on a Ni(0) complex at room temperature (rt, indicating a temperature of around 22–27 °C in this work) via ligand substitution (Fig. 1D). This mechanism for CO adsorption/desorption is based on using a multifunctional carbene ligand with a hemi-labile coordination site, whereas previously reported systems rely on the simple coordination/dissociation of CO on coordinatively unsaturated metal centers (*6*,*9*,*10*,*13*) (Fig. 1C). Furthermore, we demonstrate that the use of an ionic liquid (IL) as the reaction medium, i.e., as a dispersant and/or solvent for the adsorbents enhances the desorption effectively, which stands in sharp contrast to the typical use of ILs for the absorption of CO (*23*,*24*).

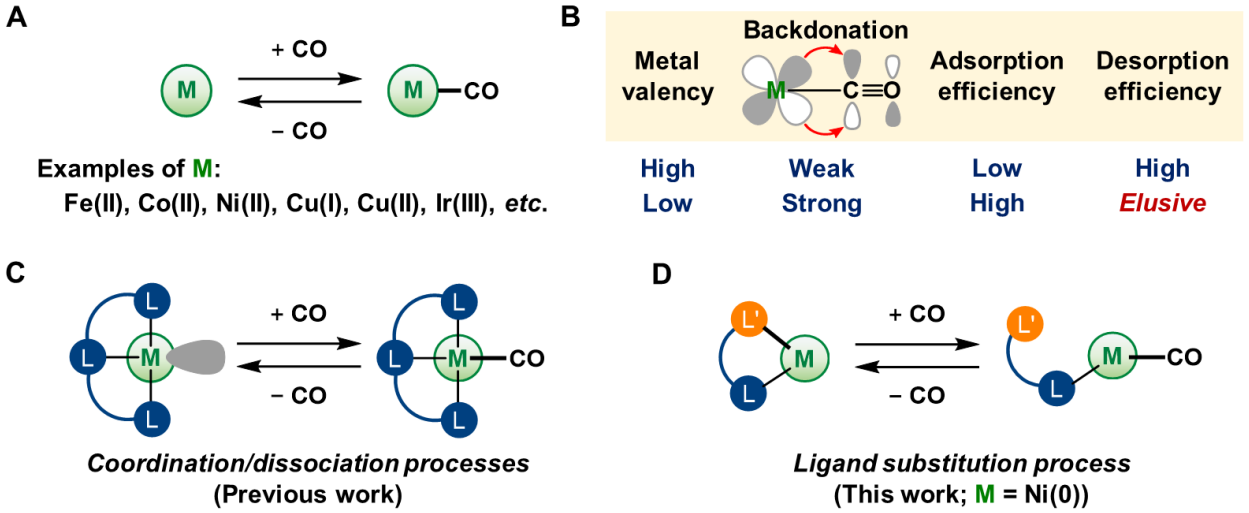

Fig. 1. Reversible chemisorption of CO using organometallic-based adsorbents. (A) Simplified scheme of the adsorption/desorption of CO on transition metals (M). (B) General comparison of the strength of M-to-CO backdonation and the efficiency of adsorption/desorption for high- and low-valent metals. (C and D) Comparison of the design strategies between previous systems using high-valent metals and the Ni(0)-based system in this work.

For the design of the Ni(0)-based system, the choice of ancillary ligand is critical. This ligand should be equipped with a hemi-labile coordination moiety that can compete with the coordination of CO to the Ni(0) centers even in the solid (crystalline) state. We thus focused on the use of *N*-phosphine-oxide-substituted imidazolylidenes (PoxIms; **1a**–**b**) and the corresponding imidazolinylidene (SPoxIm; **1c**), as the *N*-phosphinoyl group can serve as a hemi-labile ligand to coordinate Ni(0) in addition to the diaminocarbene moiety (Fig. 2A) (*25*,*26*). To date, (S)PoxIms have demonstrated various coordination modes toward metals, including coordination by only the carbene atom (*κ-C*) (*27*,*28*), by only the *N*-phosphinoyl oxygen atom (*κ-O*) (*29*,*30*), and by both the carbene and oxygen atoms (*κ-C*,*O*) (*31*,*32*); however, dynamic coordination exchange between the *κ-C* and *κ-C*,*O* modes remains unknown.

Initially, we explored a method that can selectively afford Ni(*κ-C*,*O*-**1**)$(CO)_2$ (**2**) or Ni(*κ-C*-**1**)$(CO)_3$ (**3**) (Fig. 2A). Treatment of a THF solution of PoxIm **1a**, which bears an *N*-2,6-diisopropylphenyl (Dipp) group, and Ni$(cod)_2$ with 2.2 equivalents of *ex-situ*-generated CO at rt

resulted in the formation of **2a**, which was isolated in 85% yield. The selective preparation of **3a** was achieved by using an excess of CO (ca. 8.0 eq.) at rt in toluene, and **3a** was isolated in 92% yield. The yield of **3a** slightly decreased to 70% when the reaction was carried out in THF. Similarly, di-/tri-carbonyl complexes **2b**/**3b**, which bear PoxIm **1b** with an *N*-mesityl group, and dicarbonyl complex **2c**, which bears SPoxIm **1c** with a Dipp group, were prepared in excellent yields, whereas Ni(*κ*-*C*-**1c**)$(CO)_3$ (**3c**) was isolated in 85% after recrystallization due to its rapid conversion to **2c** during the removal of volatile species *in vacuo*. These compounds were unambiguously characterized using multinuclear NMR and IR spectroscopy as well as single-crystal X-ray diffraction (SC-XRD) analysis. For example, in the ^{31}P NMR spectra, the resonance of the *N*-phosphinoyl moiety in **2a** is observed at δ_P 66.9, which represents a significant downfield shift compared to that of **3a** (δ_P 58.4). The A_1-symmetrical carbonyl stretching frequencies of **3a**/**3c** (2048–2049 cm^{-1}; in CH_2Cl_2) are nearly identical, but slightly lower than the values of Ni(*κ*-*C*-**1d**/**1e**)$(CO)_3$ (**3d**/**3e**; 2052 cm^{-1}) (*33*), where **1d** is 1,3-bis(2,6-diisopropylphenyl)imidazol-2-ylidene and **1e** is 1,3-bis(2,6-diisopropylphenyl)imidazolidin-2-ylidene, indicating a negligible difference in the electron density on their Ni(0) centers (*34*).

The molecular structures of **2a**, **2c**, **3a** and **3c** obtained from SC-XRD analysis are shown in Fig. 2B. In these cases, the C1 and O1 atoms adopt a *syn*-orientation with respect to the N–P bonds (C1-N2-P-O1 torsion angle: 5.8(2)° in **2a**; 8.5(1)° in **2c**; 1.3(3)° in **3a**; 6.5(2)° in **3c**), indicating that the complexation proceeded via the rotation of the *N*-phosphinoyl group in free **1**, wherein the C1 and O1 atoms adopt an *anti*-orientation (C-N-P-O: 175.9(1)° in **1a**; 179.7(2)° in **1c**) (*25*). The interatomic distances between Ni and O1 suggest the absence of a bonding interaction between these atoms in **3a** (3.148(2) Å) and **3c** (3.099(2) Å), while the formation of Ni–O1 bonds is clearly confirmed in **2a** (2.269(2) Å) and **2c** (2.227(1) Å). Stronger interactions are expected between the Ni and C1 atoms in **2a** (1.937(2) Å) and **2c** (1.929(2) Å) compared to those in **3a** (1.986(3) Å) and **3c** (1.977(2) Å), which can be rationalized in terms of the decreased number of π-acidic CO ligands. Ni K-edge X-ray absorption spectroscopy confirmed that the electronic states and local structures around the Ni centers are almost identical for **3a** and **3c** (Fig. S52–54). In their entirety, these results demonstrate the first example of the selective formation of Ni(0) complexes that bear two or three carbonyl ligands in the presence of a single NHC ligand.

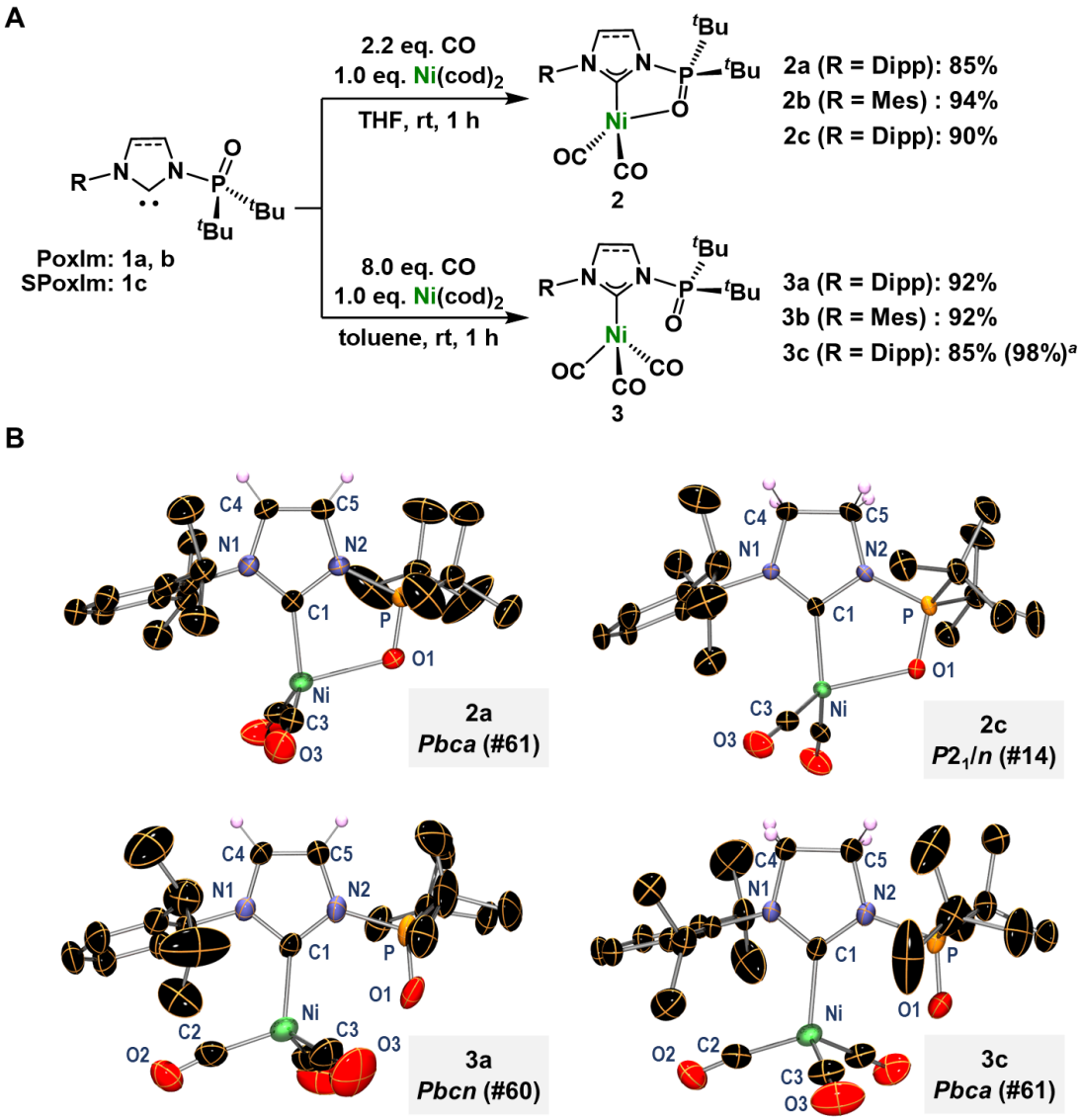

Fig. 2. Selective preparation of Ni(*κ*-*C*,*O*-1)(CO)$_2$ (2) and Ni(*κ*-*C*-1)(CO)$_3$ (3). (A) Synthesis of **2** and **3**. Isolated yields are shown. [a] NMR yield confirmed *in situ*. (B) Molecular structures of **2a**, **2c**, **3a** and **3c** with thermal ellipsoids at 30% probability; H atoms (except those bounded to C4 and C5 atoms) are omitted for clarity. Selected bond lengths/interatomic distances (Å) and angles (°) for **2a**: Ni−C1 1.937(2), Ni−C3 1.742(3), Ni−O1 2.269(2), C1-N-P-O1 5.8(2); **3a**: Ni−C1 1.986(3), Ni−C2 1.794(4), Ni−C3 1.789(5), Ni···O1 3.148(2), C1-N-P-O1 1.3(3); **2c**: Ni−C1 1.929(2), Ni−C3 1.757(2), Ni−O1 2.227(1), C1-N-P-O1 8.5(1); **3c**: Ni−C1 1.977(2), Ni−C2 1.807(3), Ni−C3 1.792(3), Ni···O1 3.099(2), C1-N-P-O1 6.5(2).

During the preparation of the aforementioned complexes, we noticed the partial formation of **2c** when a solution of **3c** was concentrated *in vacuo*. In fact, stirring the crystalline powder of **3c** at rt for 10 h *in vacuo* (0.3 mmHg) resulted in the formation of **2c** in 50% yield (Fig. 3A). Prolonging the reaction time resulted in a slight improvement in the efficiency of CO desorption from **3c** (20 h, 59%). Nevertheless, further desorption was not expected, as the solids adhered to the inner surface of the reaction vessel, limiting the surface area of **3c** exposed to the reduced

pressure even under stirring conditions (Fig. S22). To promote the desorption, we explored the use of a dispersant. Dispersing **3c** into tetradecane ($C_{14}H_{30}$) in the reaction flask (V = 50 mL) resulted in a significant improvement of the desorption, and **2c** was obtained in >99% yield after 2 h at rt with concomitant loss of the crystallinity (Fig. 3A); however, ca. 2 wt% of $C_{14}H_{30}$ was removed under the applied reaction conditions. Desorption also proceeded quantitatively within 30 minutes when **3c** was fully dissolved in 1,3-dimethoxybenzene (DMB), albeit that the partial removal of DMB (ca. 2 wt%) was again inevitable (Fig. S26).

To achieve a fully reusable and reversible chemisorption system that can produce CO of high purity, the concomitant removal of reaction media should be avoided. We thus turned our attention to the use of ionic liquids (ILs), which exhibit negligible vapor pressure. ILs including Cu(I) ions have been explored as potential CO absorbents (*24*); however, these have not yet been used as the dispersant/solvent in the desorption process, probably because ILs can occupy the pores of nanoporous materials. The dispersion of the crystalline powder of **3c** in imidazolium-based **IL-1** with the anion $OSO_2CF_3^-$ (OTf^-) (350 mg) under reduced pressure resulted in obvious improvement of the desorption to afford **2c** in 90% yield (run 1, Fig. 3B). It should be noted that the yield of **2c** was calculated via NMR analysis after the addition of THF-d_8 to the resulting mixture. We experimentally confirmed that the addition of THF-d_8 causes negligible changes to **2c** over a short period at rt; however, after 24 h, **2c** partially decomposed to give **1c·HOTf** (36%) via deprotonation of the proton at the C2 position in **IL-1** (Fig. S34). In contrast, **3c** did not show any decomposition under identical conditions.

Subsequently, we explored the optimization of the desorption conditions. The use of C2-methylated **IL-2** with the anion NTf_2^- resulted in the formation of **2c** in 98% yield by preventing the aforementioned decomposition (run 2). **IL-3** with the anion PF_6^- also exhibited good compatibility with the applied conditions, although a slight decrease in the desorption efficiency was observed (90%; run 3). In contrast, a black precipitate was immediately generated after mixing **3c** and **IL-4** with the anion $CH_3SO_4^-$, and **2c** was not formed (run 4). Thus, **IL-2** was used in the following experiments. It should be noted that up to 2.1 $\times 10^{-2}$ M of **3c** can be dissolved in **IL-2** at 25 °C, which corresponds to a 20% loading of **3c**, while **2c** shows higher solubility (6.7 $\times 10^{-2}$ M at 25 °C) (Fig. S32). Thus, a significant amount of solid **3c** remained during the initial stage of the CO desorption, while little solid was observed after the reaction had completed, as most of the formed **2c** was dissolved in **IL-2** (*vide infra*).

The loading amount of **IL-2** was optimized by comparing the average yields of **2c** obtained in five independent experiments under each loading condition (runs 5–8). When 350 mg of **IL-2** was used, an average yield of 65(3)% was confirmed (run 5), while using 100 mg of **IL-2** (run 6) furnished a yield of 54(3)%; however, this difference was not confirmed to be statistically significant. Nevertheless, the desorption efficiency significantly decreased when 500 mg (39(3)%; run 7) or 1000 mg (45(3)%; run 8) of **IL-2** was employed, even though more **3c** could be dissolved in **IL-2** under these conditions. Based on the aforementioned results, the CO desorption should occur predominantly on the dispersed solids of **3c**, and the amount of IL should influence the efficiency of its dispersion. The amount of IL should be optimized based on the reaction apparatus; accordingly, we employed 350 mg of **IL-2** in the reaction vial (V = 2.0 mL) in subsequent experiments.

Under the optimal desorption conditions using **IL-2** as the reaction medium, **3c** was converted into **2c** in 97% yield after 4 h at rt under reduced pressure (Fig. 3C). Interestingly, only 9% desorption of CO from **3a** proceeded under identical conditions (*35*), even though the geometric and electronic features of **3a** and **3c** are almost identical (*vide supra*). This significant

difference in the desorption rate could be interpreted in terms of the structural flexibility of the ancillary ligands. Complex **3b** was also subjected to identical desorption conditions, but the resulting yield of **2b** was only 19%. No reaction occurred for **3d** or **3e**. To evaluate the role of the *N*-phosphinoyl oxygen atom in **3c**, we synthesized Ni(*κ*-*C*-**1f**)$(CO)_3$ (**3f**), which underwent desorption of CO to generate Ni(*κ*-*C*,*P*-**1f**)$(CO)_2$ (**2f**) in 39% yield, where **1f** is a *N*-phosphanyl-substituted imidazolidin-2-ylidene. These results demonstrate that the hemi-labile behavior of the *N*-phosphinoyl moiety (**3c** vs **3e–f**) and the structural flexibility derived from the ethylene moiety in the imidazolidin-2-ylidene ring (**3c** vs **3a**) are both essential to achieve the efficient desorption of CO from the Ni(0) center under the applied conditions.

Then, we explored the adsorption of CO by **2** in the presence of **IL-2** at rt; this adsorption should predominantly occur in the solvated state given the sufficient solubility of complexes **2** in **IL-2** (Fig. 3D). Stirring **2a**/**2c** and 350 mg of **IL-2** under a CO/N_2 (1 atm each) atmosphere afforded **3a**/**3c** in 98% yields via the selective adsorption of CO with concomitant precipitation of fine crystals of **3** (**3c** is shown as an example in Fig. 4B). The reversible coordination of the *N*-phosphinoyl oxygen atom was again confirmed to be effective, as treatment of **2f** with CO/N_2 resulted in the formation of **3f** in 47% after 30 minutes. In addition, CO was directly stored in **3c** from gaseous mixtures of $CO/CH_4/N_2$ (1 atm each) and $CO/H_2/N_2$ (1 atm each) in excellent yields through adsorption by **2c**. Thus, the present system could also be used for the purification of CH_4 and H_2 through the removal of the accompanying CO. Ni(0) dicarbonyl complexes **2g** and **2h**, which bear a bidentate carbene (**1g**) or phosphine (**1h**) ligand, respectively, did not react with excess CO even after being dissolved in THF-d_8 (Fig. 3E). We also explored the preparation of Ni(0) dicarbonyl complexes that bear the bidentate ligands with a phosphine oxide group **1i** and **1j**. As a result, Ni(*κ*-*C*-**1i**)$_2(CO)_2$ (**4i**) and Ni(*κ*-*P*-**1j**)$_2(CO)_2$ (**4j**) were obtained even in the presence of excess CO (Fig. 3F). The results of these experiments show that our strategy based on the use of (S)PoxIm ligands and IL-based media is effective for the precise separation of CO from gaseous mixtures including N_2, H_2, and CH_4.

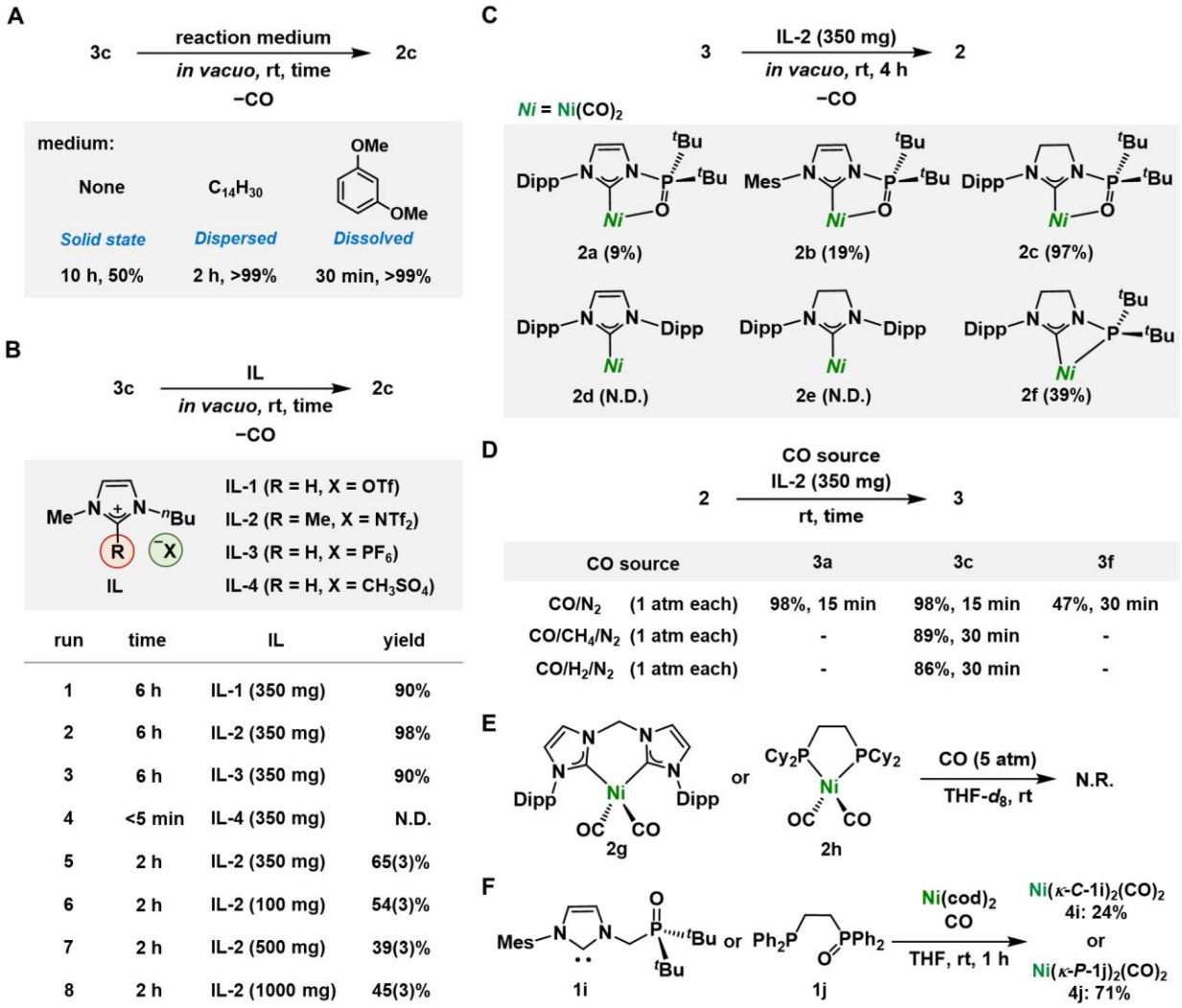

Fig. 3. Reversible chemisorption of CO on Ni(0) complexes. (A) Effect of $C_{14}H_{30}$ as a dispersant and DMB as a solvent. (B) Effect of the structure and amount of the IL. General procedure for the CO desorption: **3c** (3.0×10^{-2} mmol) was dispersed in the IL in the reaction vial under reduced pressure (0.3 mmHg), followed by the addition of THF-d_8 for NMR analysis to estimate the yield of **2c**. (C) Effect of the ligand. For the reaction from **3f**, a mixture of **3f**/**2f** (86/14) was employed. (D) Adsorption of CO by **2**. General procedure: a mixture of **2** (3.0×10^{-2} mmol) and **IL-2** (350 mg) was stirred in the reaction vial (V = 2.0 mL) at rt in the presence of a CO source, followed by the addition of THF-d_8 for NMR analysis to estimate the yield of **3**. (E) Reaction between **2g**/**2h** and CO. (F) Reaction between **1i**/**1j** and $Ni(cod)_2$ in the presence of CO (2.2 eq. for **1i**; >17 eq. for **1j**).

We then investigated the reusability of the present chemisorption system and found a significant acceleration of the rate of CO desorption between the first and second cycles (Fig. 4A). In fact, **2c** was afforded in 87–88% yield within 2 h from **3c** prepared under the optimized conditions via either the adsorption of CO on **2c** or sequential CO desorption–adsorption reactions from crystalline **3c**, whereas **2c** was obtained in 65(3)% yield from crystalline **3c** (run 5, Fig. 3B). This result can be explained by the increase in the total surface area of **3c** exposed to the reduced

pressure, as the crystals of **3c** that were re-precipitated after CO adsorption were significantly smaller than those used in the first desorption process (Fig. 4B). Furthermore, CO was effectively desorbed from **3c** even after five desorption–adsorption cycles. It should be noteworthy that **3c** can be used for the purpose of CO-storage, as solid-state **3c** and the mixture of **3c**/**IL-2** were stable for at least 7 days at rt and –30 °C, respectively (Fig. S36). In the aforementioned five cycles, the mixture of **3c**/**IL-2** was stored at –30 °C for 14–16 h after each desorption/adsorption cycle completed. These results shed light on the key features of the Ni(0)-based reversible chemisorption of CO, i.e., this system can be reused without the removal/addition of the IL, and crystallization is not essential for the preparation of the adsorbents.

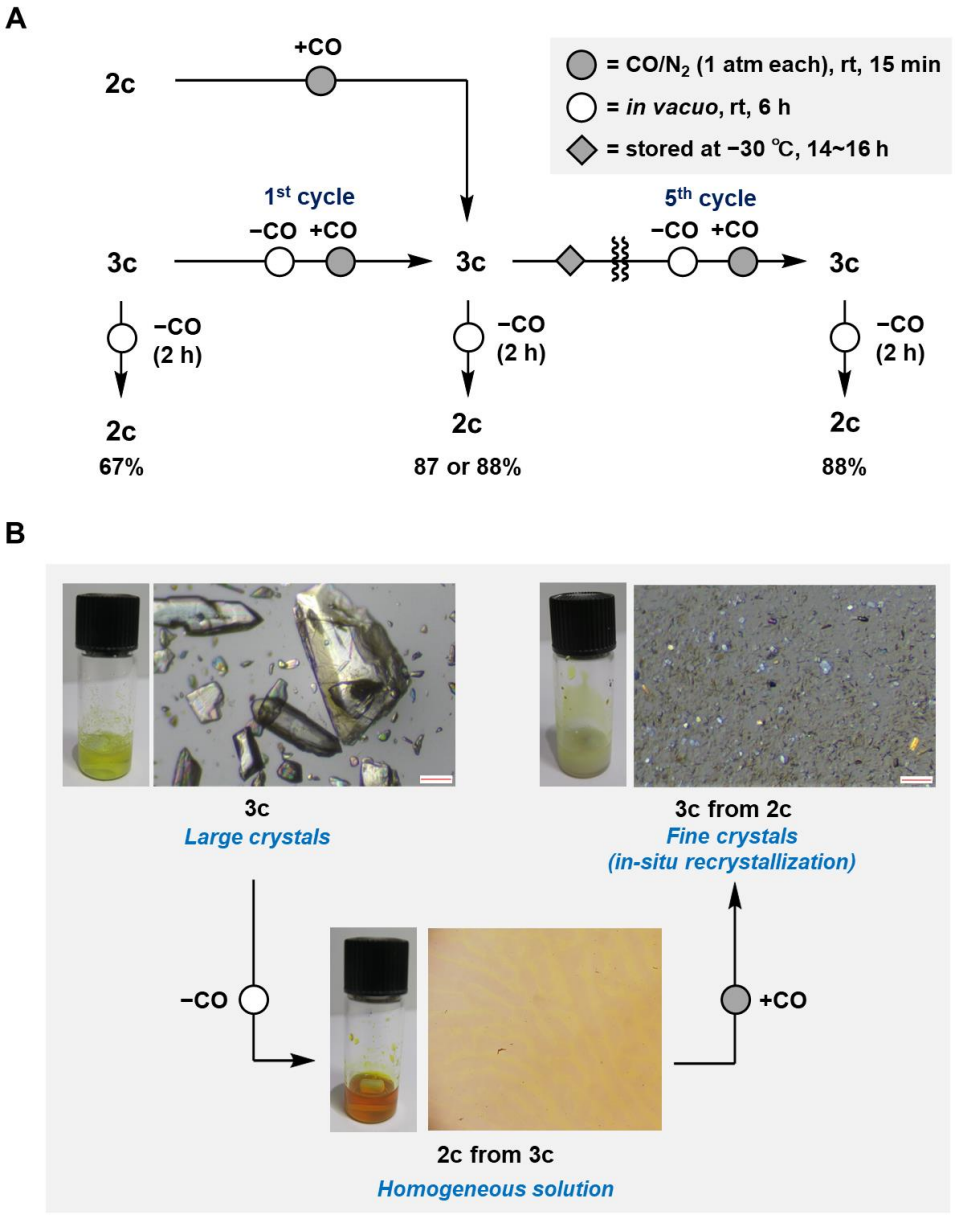

Fig. 4. Repeated use of the present CO chemisorption system. (A) Five cycles of repeated CO adsorption/desorption with **IL-2** (350 mg). (B) Photographs and micrographs of reaction samples during the 1st cycle of CO desorption from **3c** to give **2c** and subsequent CO adsorption to again furnish **3c**. The scale-bar shown in red is equivalent to 3.0 mm.

To clarify the reason for the obvious difference in the CO desorption rates of **3a** and **3c**, density functional theory (DFT) calculations were carried out at the *ω*B97X-D/Def2-TZVPD//M06-L/Def2-SVPD (for Ni and O) and Def2-SVP for others//gas phase level of theory. First, we identified two plausible pathways that connect **3c** and **2c**; in the first, the C2≡O2 moiety at the distal position with respect to the *N*-phosphinoyl oxygen atom dissociates from **3c**, while in the second, the C3≡O3 moiety at the proximal position dissociates (for atomic labels, see Fig. 5B. For details of these two pathways, see Fig. S40). A significant difference in the activation energy barriers ($\Delta G^{\ddagger}$) of these pathways was observed (+13.3 kcal mol^{-1} for the former; +17.0 kcal mol^{-1} for the latter), indicating that the dissociation of CO from **3c** should proceed via cleavage of the C2–Ni bond (Fig. 5A). In the optimized structure of **TS1c** shown in Fig. 5B, the interatomic distance between Ni and O1 is shortened to 2.53 Å from the 3.14 Å found in the optimized structure of **3c**, while the distance between Ni and C2 is elongated to 2.73 Å from 1.82 Å in **3c**. Although these results are based on the structures optimized in the gas phase, the transformation of **3c** to **2c** should proceed via ligand substitution even under the applied experimental conditions. This ligand substitution results in the formation of the intermediate **[2c···CO]** (ΔG° = +12.9 kcal mol^{-1} with respect to **3c**). The **2c** moiety in **[2c···CO]** exhibits a geometry that is nearly identical to that of the optimized **2c**, e.g., the Ni–O1 lengths are 2.31 Å in **[2c···CO]** and 2.30 Å in **2c**.

Next, the activation energy barriers for the dissociation of CO from the Ni(0) centers of **3a**, **3c**, and **3f** were compared (Fig. 5A). The values of $\Delta G^{\ddagger}$ (with respect to that of **3**) increase in the order **TS1c** (+13.3 kcal mol^{-1}) < **TS1f** (+14.2 kcal mol^{-1}) < **TS1a** (+14.9 kcal mol^{-1}). This trend is consistent with the experimental results that show that the efficiency of CO desorption increases in the order **3a** (9%) < **3f** (39%) < **3c** (97%) under the applied experimental conditions (Fig. 3C). The presence of the *N*-phosphinoyl oxygen atom in **3c** minimizes the change in the spatial environment around the Ni(0) center during the CO substitution process, which was evaluated using the percent buried volume (%V_{bur}) calculated based on the geometrical parameters obtained from DFT calculations (*36*,*37*). The change in %V_{bur} (Δ%V_{bur}) (*26*) was found to be 3.3 when the %V_{bur} values of the **1c** moieties in **3c**, **TS1c**, and **[2c···CO]** were compared; this value is obviously smaller than the Δ%V_{bur} of 7.5 calculated for the transformation of **3f** into **[2f···CO]** via **TS1f**, thus rationalizing the faster interconversion in the former case compared to that of the latter.

A comparison of the coordinates of the Ni, C5, C6, P, and O1 atoms between **3** and **TS1** reveals that larger deviations are generated in these atoms during the transformation from **3c** to **TS1c** than during that from **3a** to **TS1a**, highlighting the enhanced flexibility of the skeleton of **1c** (Fig. 5C). The C2, Ni, and O1 atoms in **3c** can thus smoothly adopt a suitable orientation for the ligand substitution by reducing the Ni···O1 distance by 0.61 Å to reach **TS1c**. In contrast, in the case of the formation of **TS1a** from **3a**, the Ni···O1 distance must be shortened by 0.69 Å under more structurally restricted conditions, resulting in a larger $\Delta G^{\ddagger}$ to reach **TS1a**.

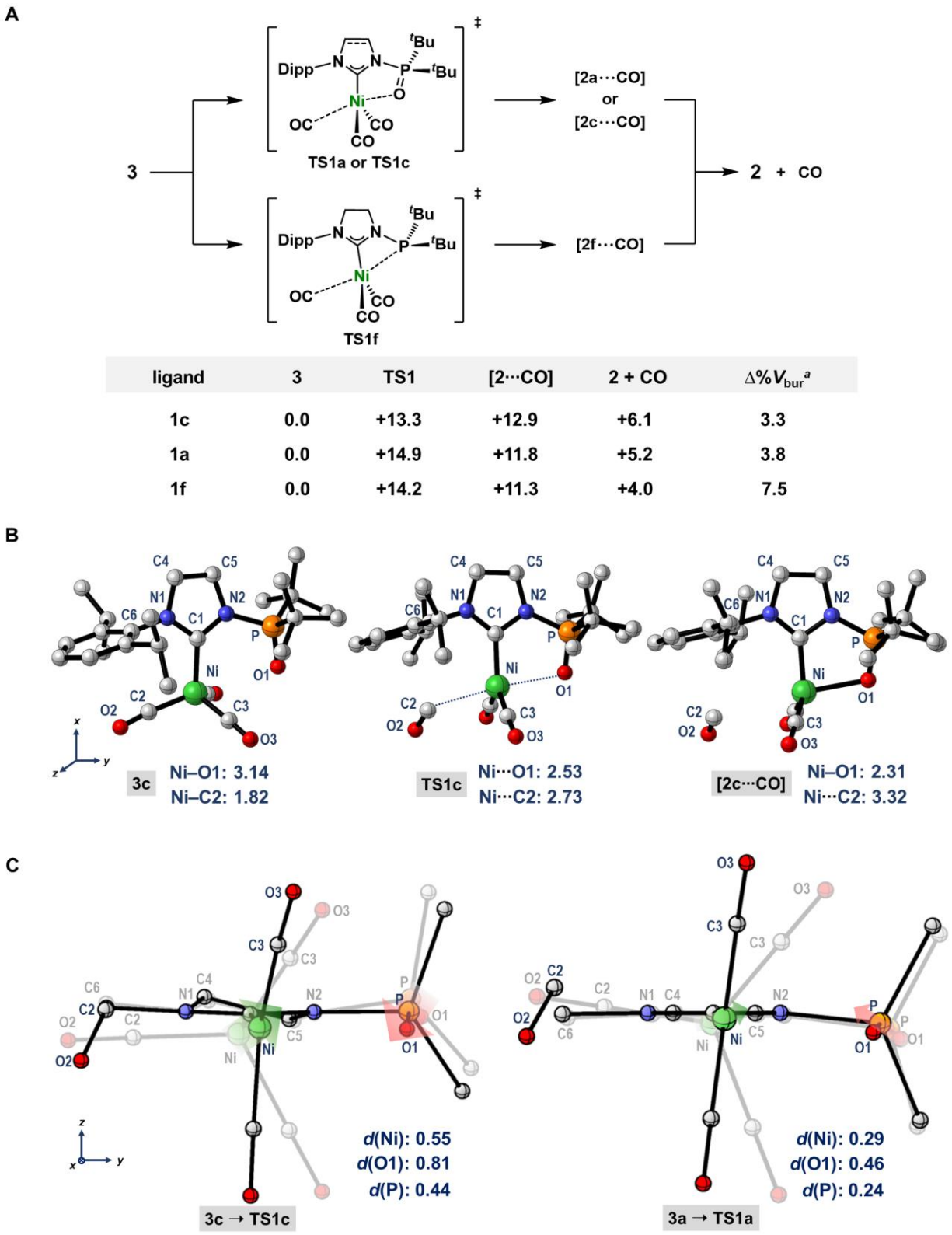

ligand	3	TS1	[2···CO]	2 + CO	$\Delta\%V_{bur}$ [a]
1c	0.0	+13.3	+12.9	+6.1	3.3
1a	0.0	+14.9	+11.8	+5.2	3.8
1f	0.0	+14.2	+11.3	+4.0	7.5

Fig. 5. Theoretical studies. (A) Plausible reaction pathways for the interconversion between **3** and **2**, calculated at the ωB97X-D/Def2-TZVPD//M06-L/Def2-SVPD (for O and Ni) and Def2-SVP (for all other atoms) level of theory (gas-phase, 298.15 K, 1 atm). Relative Gibbs energies (kcal mol^{-1}) are given with respect to **3** (+0.0 kcal mol^{-1}). $\%V_{bur}$ values calculated using the

program Samb*V*ca (r = 3.5 Å; d = 2.0 Å; bondi radii scaled by 1.17; H atoms are omitted) based on the structural parameters optimized by DFT calculations: **3c**, 40.5; **TS1c**, 43.6; **[2c···CO]**, 43.8; **2c**, 45.2; **3a**, 40.2; **TS1a**, 43.5; **[2a···CO]**, 44.0; **2a**, 42.7; **3f**, 39.1; **TS1f**, 43.6; **[2f···CO]**, 46.6; **2f**, 46.9. [a] $\Delta\%V_{bur}$ is the difference between the maximum and minimum $\%V_{bur}$ values obtained for **3**, **TS1**, and **[2···CO]**. (B) Optimized gas-phase structures of **1c**, **TS1c**, and **[2c···CO]**. Selected bond lengths (Å) are shown. (C) Comparison of the geometric deviations generated during the transformations from **3c** to **TS1c** (left) and from **3a** to **TS1a** (right). The structures for each **3**/**TS1** pair are overlaid with respect to their N1-Ni-N2 planes. The deviation distances (Å) for the Ni, O1, and P atoms are also shown.

The reported monodentate NHCs yielded either nickel dicarbonyl (e.g., **2k**–**l**) or tricarbonyl (e.g., **3d**–**e** and **3m**–**p**) complexes, depending on their steric demand when a single molecule of NHC was treated with a Ni(0) species (Fig. 6) (*33*, *38-40*). Interestingly, $\%V_{bur}$ values of around 39.5–40.0 seem to represent a plausible boundary that determines whether di- or tri-carbonyl complexes are generated as isolable species. In this context, (S)PoxIms **1a**–**c** and *N*-phosphanyl-substituted **1f** demonstrate unprecedented reactivity to afford both di- and tri-carbonyl complexes and realize their interconversion beyond the possible boundary of $\%V_{bur}$ by effectively scaling the spatial volume around the Ni center.

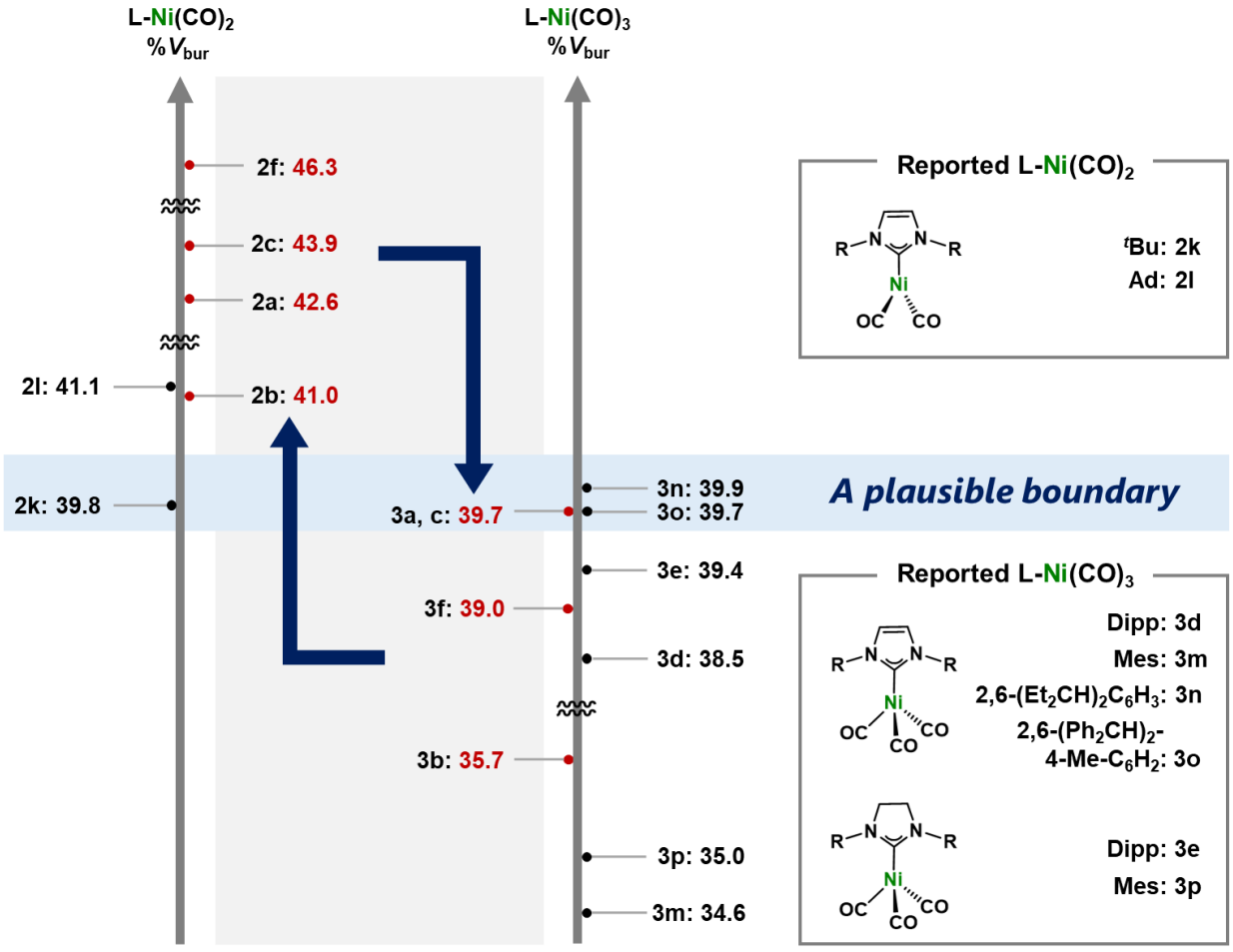

Fig. 6. A plausible $\%V_{bur}$ boundary for the formation of Ni(0) di- or tri-carbonyl complexes that bear NHCs. The $\%V_{bur}$ values were calculated based on the geometric parameters obtained

from the SC-XRD analysis, reported in this work (**2a**–**c**, **2f**, **3a**–**c** and **3f**) and the previous works (**2k**–**l**, **3d**–**e** and **3m**–**p**) (*33, 38-40*).

The presented preliminary results serve as proof-of-concept for a reusable and reversible chemisorption system for CO based on the use of zero-valent transition-metal complexes at room temperature driven only by pressure-swing manipulation. We believe that the strategy shown in this work, i.e., (i) the construction of a ligand system that functions even in the solid-state for the reversible CO substitution using flexible multifunctional ligands and (ii) the use of an ionic liquid as the reaction medium, will pave the way for the design of an unprecedented molecular-based chemisorption system that can effectively purify (or remove) CO in a low-energy-consuming and sustainable manner.

References and Notes

1. H.-W. Häring, Ed., *Industrial Gases Processing* (Wiley–VCH: Weinheim, 2008).
2. L. Mond, C. Langer, F. Quincke, L.-Action of Carbon Monoxide on Nickel. *J. Chem. Soc., Trans.* **57**, 749–753 (1890).
3. A. Morrison, J. J. Leitch, G. Szymanski, G. Moula, B. Barlow, I. J. Burgess, B. Shobeir, H. Huang, J. Lipkowski, *Electrochimica Acta* **260**, 684–694 (2018).
4. Á. A. Ramrírez-Santos, C. Castel, E. Favre, A review of gas separation technologies within emission reduction programs in the iron and steel sector: Current application and development perspectives. *Sep. Purif. Technol.* **194**, 425–442 (2018).
5. A. Evans, R. Luebke, C. Petit, The use of metal–organic frameworks for CO purification. *J. Mater. Chem. A* **6**, 10570–10594 (2018).
6. D. Benito-Garagorri, M. Puchberger, K. Mereiter, K. Kirchner, Stereospecific and Reversible CO Binding at Iron Pincer Complexes. *Angew. Chem. Int. Ed.* **47**, 9142–9145 (2008).
7. D. Benito-Garagorri, I. Lagoja, L. F. Veiros, K. A. Kirchner, Reactivity of coordinatively unsaturated iron complexes towards carbon monoxide: to bind or not to bind? *Dalton Trans.* **40**, 4778–4792 (2011).
8. C. W. Tate, A. deMello, A. D. Gee, S. Kealey, R. Vilar, A. J. P. White, N. J. Long, Hemilabile and reversible carbon monoxide binding properties of iron(II), cobalt(II) and nickel(II) complexes containing a new tridentate P–S–N ligand. *Dalton Trans.* **41**, 83–89 (2012).
9. A. T. Gallagher, C. D. Malliakas, T. D. Harris, CO Binding at a Four-Coordinate Cobaltous Porphyrin Site in a Metal−Organic Framework: Structural, EPR, and Gas Adsorption Analysis. *Inorg. Chem.* **56**, 4654−4661 (2017).
10. E. D. Bloch, M. R. Hudson, J. A. Mason, S. Chavan, V. Crocellà, J. D. Howe, K. Lee, A. L. Dzubak, W. L. Queen, J. M. Zadrozny, S. J. Geier, L.-C. Lin, L. Gagliardi, B. Smit, J. B. Neaton, S. Bordiga, C. M. Brown, J. R. Long, Reversible CO Binding Enables Tunable CO/H_2 and CO/N_2 Separations in Metal−Organic Frameworks with Exposed Divalent Metal Cations. *J. Am. Chem. Soc.* **136**, 10752−10761 (2014).
11. C. W. Tate, A. D. Gee, R. Vilar, A. J. P. White, N. J. Long, Reversible carbon monoxide binding at copper(I) P–S–X (X = N, O) coordination polymers. *J. Organomet. Chem.* **715**, 39−42 (2012).
12. H. Sato, W. Kosaka, R. Matsuda, A. Hori, Y. Hijikata, R. V. Belosludov, S. Sakaki, M. Takata, S. Kitagawa, Self-Accelerating CO Sorption in a Soft Nanoporous Crystal. *Science* **343**, 167−170 (2014).
13. L.-Y. Sun, Y.-Y. An, L.-L. Ma, Y.-F. Han, Single-Crystalline Organoiridium Complex for Gas-

Triggered Chromogenic Switches and Its Applications on CO Detection and Reversible Scavenging. *Chin. J. Chem.* **37**, 763−768 (2019).
14. T. Islamoglu, Z. Chen, M. C. Wasson, C. T. Buru, K. O. Kirlikovali, U. Afrin, M. R. Mian, O. K. Farha, Metal−Organic Frameworks against Toxic Chemicals. *Chem. Rev.* **120**, 8130−8160 (2020).
15. D. A. Reed, D. J. Xiao, M. I. Gonzalez, L. E. Darago, Z. R. Herm, F. Grandjean, J. R. Long, Reversible CO Scavenging via Adsorbate-Dependent Spin State Transitions in an Iron(II)−Triazolate Metal−Organic Framework. *J. Am. Chem. Soc.* **138**, 5594−5602 (2016).
16. H. Hirai, K. Wada, M. Komiyama, Active Carbon-Supported Copper(I) Chloride as Solid Adsorbent for Carbon Monoxide. *Bull. Chem. Soc. Jpn.* **59**, 2217–2223 (1986).
17. M. E. Moragues, J. Esteban, J. V. Ros-Lis, R. Martínez-Mánez, M. D. Marcos, M. Martínez, J. Soto, F. Sancenón, Sensitive and Selective Chromogenic Sensing of Carbon Monoxide via Reversible Axial CO Coordination in Binuclear Rhodium Complexes. *J. Am. Chem. Soc.* **133**, 15762–15772 (2011).
18. K. J. Balkus, Jr., A. Kortz, R. S. Drago, Carbon Monoxide Binding by Copper(I) Complexes Supported on Polystyrene. *Inorg. Chem.* **27**, 2955−2958 (1988).
19. J. I. Dulebohn, S. C. Haefner, K. A. Berglund, K. R. Dunbar, Reversible Carbon Monoxide Addition to Sol-Gel Derived Composite Films Containing a Cationic Rhodium(I) Complex: Toward the Development of a New Class of Molecule-Based CO Sensors. *Chem. Mater.* **4**, 506−508 (1992).
20. *Materials for Separation Technologies: Energy and Emission Reduction Opportunities* (Oak Ridge National Laboratory, U. S. Department of Energy, 2005).
21. L. S. Sunderlin, D. Wang, R. R. Squires, Metal Carbonyl Bond Strengths in $Fe(CO)_n^-$ and $Ni(CO)_n^-$. *J. Am. Chem. Soc.* **114**, 2788−2796 (1992).
22. M. Zhou, L. Andrews, C. W. Bauschlicher, Jr., Spectroscopic and Theoretical Investigations of Vibrational Frequencies in Binary Unsaturated Transition-Metal Carbonyl Cations, Neutrals, and Anions. *Chem. Rev.* **101**, 1931−1962 (2001).
23. S. Raeissi, L. J. Florusse, C. J. Peters, Purification of Flue Gas by Ionic Liquids: Carbon Monoxide Capture in [bmim][Tf_2N]. *AIChE J.* **59**, 3886−3891 (2013).
24. Z.-H. Tu, Y.-Y. Zhang, Y.-T. Wu, X.-B. Hu, Self-enhancement of CO reversible absorption accompanied by phase transition in protic chlorocuprate ionic liquids for effective CO separation from N_2. *Chem. Commun.* **55**, 3390−3393 (2019).
25. Y. Hoshimoto, T. Kinoshita, M. Ohashi, S. Ogoshi, A Strategy to Control the Reactivation of Frustrated Lewis Pairs from Shelf-Stable Carbene Borane Complexes. *Angew. Chem. Int. Ed.* **54**, 11666–11671 (2015).
26. Y. Hoshimoto, S. Ogoshi, Development of Metal Complexes Equipped with Structurally Flexible Carbenes. *Bull. Chem. Soc. Jpn.* **94**, 327–338 (2021).
27. L. Branzi, M. Baron, L. Armelao, M. Rancan, P. Sgarbossa, C. Graiff, A. Pöthig, A. Biffis, Coordination chemistry of gold with *N*-phosphine oxide-substituted imidazolylidenes (POxIms). *New J. Chem.* **43**, 17275–17283 (2019).
28. T. Asada, Y. Hoshimoto, S. Ogoshi, Rotation-Triggered Transmetalation on a Heterobimetallic Cu/Al *N*-Phosphine-Oxide-Substituted Imidazolylidene Complex. *J. Am. Chem. Soc.* **142**, 9772−9784 (2020).
29. T. Kinoshita, M. Sakuraba, Y. Hoshimoto, S. Ogoshi, Complexation between MOTf (M = Li and Na) and *N*-Phosphine Oxide-substituted Imidazolylidenes via Coordination of the *N*-Phosphoryl Groups. *Chem. Lett.* **48**, 230–233 (2019).
30. T. Asada, Y. Hoshimoto, T. Kawakita, T. Kinoshita, S. Ogoshi, Axial Chirality around N−P Bonds Induced by Complexation between $E(C_6F_5)_3$ (E = B, Al) and an *N*-Phosphine Oxide-

Substituted Imidazolinylidene: A Key Intermediate in the Catalytic Phosphinoylation of CO_2. *J. Org. Chem.* **85**, 14333−14341 (2020).
31. W. Tao, S. Akita, R. Nakano, S. Ito, Y. Hoshimoto, S. Ogoshi, K. Nozaki, Copolymerisation of ethylene with polar monomers by using palladium catalysts bearing an N-heterocyclic carbene–phosphine oxide bidentate ligand. *Chem. Commun.* **53**, 2630−2633 (2017).
32. L. Branzi, D. Franco, M. Baron, L. Armelao, M. Rancan, P. Sgarbossa, A. Biffis, Palladium(II) Complexes with *N*-Phosphine Oxide-Substituted Imidazolylidenes (PoxIms): Coordination Chemistry and Catalysis. *Organometallics* **38**, 2298−2306 (2019).
33. R. Dorta, E. D. Stevens, N. M. Scott, C. Costabile, L. Cavallo, C. D. Hoff, S. P. Nolan, Steric and Electronic Properties of N-Heterocyclic Carbenes (NHC): A Detailed Study on Their Interaction with $Ni(CO)_4$. *J. Am. Chem. Soc.* **127**, 2485–2495 (2005).
34. We evaluated the σ-donor/π-acceptor ability of (S)PoxIms using several spectroscopic techniques (for details, see the Supplementary Materials). The results imply that (i) the σ-donor/π-acceptor ability of SPoxIm is higher than that of PoxIm (e.g., **1c** vs **1a**), and (ii) (S)PoxIms exhibit higher π-accepting properties and slightly lower σ-donating properties compared to commonly used *N*-heterocyclic carbenes such as **1d** and **1e**.
35. When the desorption of CO was carried out from the fully-dissolved states of **3a** and **3f** using a far larger amount of **IL-2** (>4 g), **2a** and **2f** were obtained in 20 and 47% yield, respectively. In the case of full-dispersion experiments using $C_{14}H_{30}$ (200 mg), **2a** and **2f** were obtained in 10 and 73% yield, respectively. These results support the conclusion that the CO desorption from **3a** and **3f** predominantly proceeds in their solid states under the applied conditions.
36. A. Gómez-Suárez, D. J. Nelson, S. P. Nolan, Quantifying and understanding the steric properties of *N*-heterocyclic carbenes. *Chem. Commun.* **53**, 2650−2660 (2017).
37. L. Falivene, Z. Cao, A. Petta, L. Serra, A. Poater, R. Oliva, V. Scarano, L. Cavallo, Towards the online computer-aided design of catalytic pockets. *Nat. Chem.* **11**, 872–879 (2019).
38. R. Dorta, E. D. Stevens, C. D. Hoff, S. P. Nolan, Stable, Three-Coordinate $Ni(CO)_2$(NHC) (NHC = *N*-Heterocyclic Carbene) Complexes Enabling the Determination of Ni−NHC Bond Energies *J. Am. Chem. Soc.* **125**, 10490−10491 (2003).
39. A. Collado, J. Balogh, S. Meiries, A. M. Z. Slawin, L. Falivene, L. Cavallo, S. P. Nolan, Steric and Electronic Parameters of a Bulky yet Flexible N-Heterocyclic Carbene: 1,3-Bis(2,6-bis(1-ethylpropyl)phenyl)imidazol-2-ylidene (IPent). *Organometallics* **32**, 3249–3252 (2013).
40. J. Balogh, A. M. Z. Slawin, S. P. Nolan, Bulky *N*-Heterocyclic Carbene IPr* in Selected Organo- and Transition Metal-Mediated Catalytic Applications, *Organometallics* **31**, 3259–3263 (2012).

Acknowledgments

Ni K-edge XAS measurements were performed at the BL14B2 beamline of SPring-8 with the approval of the Japan Synchrotron Radiation Research Institute (JASRI) (Proposal Nos. 2021A1630 and 2021B1717). Part of the computational work was performed at the Research Center for Computational Science (RCCS), Okazaki, Japan.

Funding: This project was supported by Grants-in-Aid for Scientific Research (C) (JSPS KAKENHI Grant 21K05070 for Y.H.) and for Young Scientists (JSPS KAKENHI Grant 20K15279 for Y.U.), the Environment Research and Technology Development Fund (JPMEERF20211R01) of the Environmental Restoration and Conservation Agency of Japan (Y.H.), a Mitsubishi Gas Chemical Award in Synthetic Organic Chemistry, Japan (Y.U.), and the RIKEN-Osaka University Science and Technology Hub Collaborative Research Program from

RIKEN and Osaka University (Y.U.). A part of this work was supported by JST SPRING, Grant Number JPMJSP2138 (Y.Y.).

Author contributions: Y.H. conceived and designed the experiments. Y.H., Y.Y., T.Ka., and T.Ki. performed the synthesis of materials and chemisorption experiments. Y.H. performed the computational analysis. Y.U. conducted XAS experiments. Y.H. and Y.Y. prepared an earlier version of the manuscript, which was finalized by all authors. Y.H. and S.O. directed the research.

Competing interests: The authors declare no competing interests.